

QSAR studies on CCR2 antagonists with chiral sensitive hologram descriptors

Pramod C. Nair, K. Srikanth and M. Elizabeth Sobhia*

*Centre for Pharmacoinformatics, National Institute of Pharmaceutical Education and Research (NIPER),
Sector 67, S.A.S. Nagar, Punjab 160062, India*

Received 17 September 2007; revised 18 December 2007; accepted 8 January 2008
Available online 11 January 2008

Abstract—Chemokines are small molecular weight water-soluble proteins playing a key role in immunomodulation and host-defense mechanisms. CCR2 receptor is targeted for diseases like arthritis, multiple sclerosis, vascular disease, obesity, and type 2 diabetes. Reported, herein are the QSAR studies performed on a diverse set of enantiopure analogues reported as CCR2 antagonists by hologram analysis. The best model highlights the importance of chirality feature in comparison with the other models developed without the chirality. The validated model showed high internal and external predictive power. The robustness of the model was achieved with good statistical r^2 of 0.945 and cross-validated r_{cv}^2 of 0.837. The challenging test predictivity of the model was confirmed with r_{pred}^2 of 0.807. The fragment fingerprints help in understanding essential pharmacophoric features for CCR2 antagonism and provide basis for SAR of the molecules. The 2D contribution maps with fragment information will be useful for the design of novel CCR2 antagonists having improved efficacy.

© 2008 Elsevier Ltd. All rights reserved.

Chemokines are small molecular weight water-soluble proteins playing a key role in immunomodulation and host-defense mechanisms. They selectively recruit monocytes, lymphocytes and granulocytes like neutrophils to sites of vascular injury, and inflammation.^{1–3} About 50 human chemokines are known and divided into four families based on the differences in their structure and function.² Their structural classification is based on their distinctiveness such as small size and the occurrence of four cysteine residues in conserved locations forming their 3-dimensional shape. CC chemokines fall under the largest family of chemokines and are named in such a way that the first two of the four cysteine residues in these molecules are next to each other.² They are encoded on chromosome 17 and attract mononuclear cells to sites of chronic inflammation.^{1–3} The CC family consists of several CC receptors of which CCR2 is the primary receptor for Monocyte Chemoattractant Protein-1 (MCP-1), the most characterized protein, also known as ‘chemokine ligand CCL2’. Binding of CCL2 to CCR2 triggers a number of responses including intracellular calcium mobilization, cytoskeletal rearrangement, MAP kinase activation, chemotaxis, and

degranulation.^{4,5} CCL2 and CCR2 knockout mice under a broad range of stimuli show deficient monocyte recruitment thus suggesting its potential role in inflammation.² Recently researchers have also found that obesity and insulin resistance are linked by CCL2 which induces inflammatory response (macrophage infiltration) in fatty tissues.^{3,6,7} All these studies indicate the potential role of CCL2 in obesity, diabetes, and other disease conditions linked via an inflammatory pathway.^{3,6–8}

As there is no crystal structure information available for CCR2 we have adopted ligand-based approach which is more valuable in the present study. QSAR studies are more often used as a tool for lead optimization within the congeneric domain of molecules, but there are reports of its applicability in diverse chemical space for identifying leads.^{9–13} Chirality is one of the primary aspects showing influence on the properties of compounds. And often different biological activities are exhibited for compounds with same structural formulas. Here we report the results of holographic QSAR studies performed on diverse set of chiral CCR2 antagonists. The primary objective of the present study is to develop a robust HQSAR model for predicting the CCR2 antagonistic activity for the molecules with similar descriptor properties and to explore the fragment features to gain insight into CCR2 antagonism.

Keywords: Chemokines; Enantiopure; CCR2; HQSAR; Fragments.

* Corresponding author. Tel.: +91 172 2211343; fax: +91 172 2214692; e-mail: mesophia@niper.ac.in

In vitro inhibitory activity data (IC_{50} nM) of CCR2 antagonists reported by Merck Laboratories were taken for the study. The dataset includes molecules of different structural classes including 4-amino-2-alkylbutyramides, 3,5-bis(trifluoromethyl) benzyl L-arylglutcinamide, α -aminothiazole- γ -aminobutanoic amides, and 3-amino-1-alkyl-cyclopentane carboxamides.^{14–17} Antagonistic activity data on human monocytes or CHO cells expressing human CCR2b (hCCR2b) were used for QSAR model development.^{14–17} Out of reported compounds only 50 molecules with the definite IC_{50} (nM) were taken into account and percentage data were ignored. Also the racemates were disregarded from the QSAR analysis. The dataset with 50 molecules was segregated randomly into training and test set comprising 37 and 13, respectively. (Tables 1a–1h) The IC_{50} (nM) values were taken in molar (M) range and converted to pIC_{50} according to the formula given in Eq. 1.

$$pIC_{50} = -\log IC_{50} \quad (1)$$

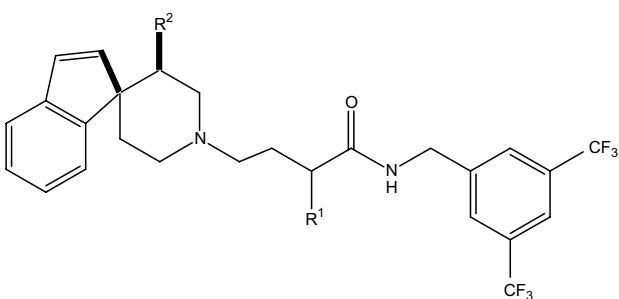
Molecular modeling studies were performed using the molecular modeling package SYBYL7.1¹⁸ installed on a Silicon Graphics Fuel Workstation running on IRIX 6.5. The structures were sketched and minimized individually by using Powell's conjugate gradient method.¹⁹

Hologram QSAR (HQSAR) is a technique which employs fragment fingerprints or molecular holograms as predictive variables of biological activity or other structurally related data.¹⁸ Fragments with different atom counts were generated and fragments with 4–7 atoms (best in our case) were hashed into bins 1–85 of the fingerprint. The bins contain information about the num-

ber of fragments hashed into each bin. The optimal HQSAR model was derived from screening through the 12 default HL values, which were a set of 12 prime numbers ranging from 53 to 401.

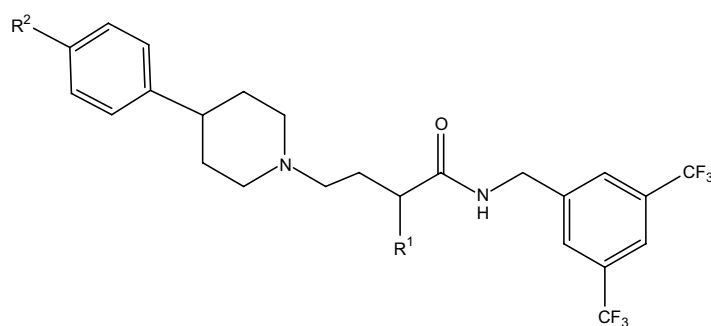
During the model development stage the first condition is to check the statistical features of the models based on the fragment size. The fragment size refers to the minimum and maximum length of the fragment in a hologram fingerprint. The statistical parameters obtained for models with different atom counts are shown in Table 2. The model with atom count 4–7 showed a high statistical value with r^2_{ncv} of 0.863 and r^2_{cv} of 0.761 when compared with other models. The second condition for model development was to distinguish molecular fragments based on their atoms, bonds, connections, chirality, hydrogens, and donor or acceptor. The model with atom count 4–7 was further scrutinized with these parameters. The atom feature enables fragment determination based on elemental atom types while the bonds and connections consider the bond orders and hybridization states within fragments, respectively. The default parameters namely atoms, bonds, and connections were tried first for the model development which gave an r^2 of 0.863 with a standard error (SE) of 0.345 holding low predictive power. (Table 2) Chirality feature which distinguishes the molecule based on its atomic and bond stereochemistry showed a remarkable thrust toward the r^2 with a value of 0.945, cross validated r^2_{cv} of 0.837, and limiting SE to 0.227. In the current study the hologram chirality parameter appropriately distinguished the R-enantiomers from their S counterparts. Other parameters excluding chirality in combination with the three default parameters gave low statistical results suggesting the poor quality models. (Table 3) Thus,

Table 1a. Structure with actual and predicted activity of alkyl-butylamide class of compounds

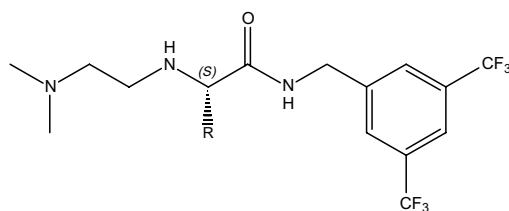


S. No.	Molecule	R ¹	R ²	IC ₅₀ (nM)	Actual pIC ₅₀	Predicted pIC ₅₀	Residual
1	1*	H	H	570	6.24	6.34	−0.10
2	2	Methyl	H	231	6.64	6.54	0.10
3	3	Methyl	H	605	6.22	6.42	−0.20
4	4	Allyl	H	193	6.71	6.59	0.12
5	5*	<i>i</i> -Propyl	H	204	6.69	6.80	−0.11
6	6	<i>i</i> -Propyl	H	349	6.46	6.59	−0.13
7	7	<i>c</i> -Propyl	H	98	7.01	6.80	0.21
8	8	H	Methyl	173	6.67	7.00	−0.33
9	9	<i>c</i> -Propyl	Methyl	14	7.85	7.49	0.36
10	10	<i>c</i> -Propyl	Methyl	80	7.10	7.23	−0.13
11	11	<i>c</i> -Butyl	Methyl	28	7.55	7.43	0.12
12	12*	<i>c</i> -Propylmethyl	Methyl	25	7.60	7.15	0.45

* Test set molecules.

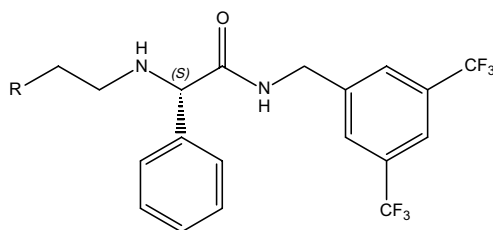
Table 1b. Structure with actual and predicted activity of alkyl-butylamide class of compounds

S. No.	Molecule	R ¹	R ²	IC ₅₀ (nM)	Actual pIC ₅₀	Predicted pIC ₅₀	Residual
13	13	<i>c</i> -Propyl	F	280	6.55	6.74	−0.19
14	14	<i>c</i> -Propyl	H	285	6.54	6.65	−0.11
15	15	<i>n</i> -Propyl	H	126	6.90	6.45	0.45
16	16	Allyl	H	642	6.19	6.43	−0.24

Table 1c. Structure with actual and predicted activity of arylglycinamide class of compounds

S. No.	Molecule	Stereo-isomer	R	IC ₅₀ (nM)	Actual pIC ₅₀	Predicted pIC ₅₀	Residual
17	17	S	4-F-Ph	770	6.11	5.98	0.13
18	18 *	S	Ph	1000	6.00	5.77	0.23
19	19 *	S	2-Thiophene	865	6.06	6.47	−0.41
20	20	S	3-Thiophene	424	6.37	6.49	−0.12

* Test set molecules.

Table 1d. Structure with actual and predicted activity of arylglycinamide class of compounds

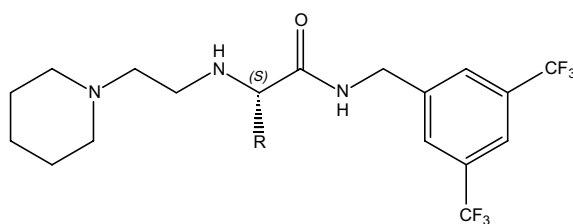
S. No.	Molecule	Stereo-isomer	R	IC ₅₀ (nM)	Actual pIC ₅₀	Predicted pIC ₅₀	Residual
21	21	S	1-Homopiperidinyl	400	6.40	6.59	−0.19
22	22 *	S	2-Me-1-piperidinyl	838	6.08	6.75	−0.67
23	23 *	S	4-Me-1-piperidinyl	756	6.12	6.83	−0.71
24	24	S	4-Ph-1-piperidinyl	822	6.08	6.04	0.04

* Test set molecules.

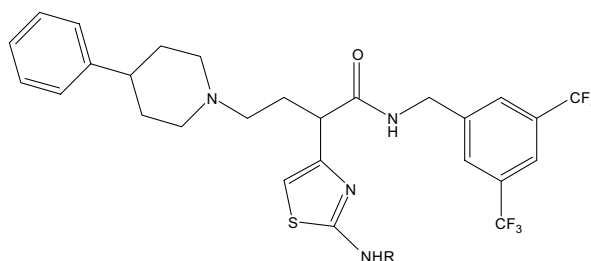
the model with chirality and three default parameters was considered as the best model.

The validation of model depends on statistical parameters such as non cross validated r^2 , cross val-

idated r^2 by Leave One Out (LOO), predictive r^2 , and standard error. The robustness of the model further relies on the more challenging external test prediction reflected by its predictive r^2 value. Like r^2_{cv} , the predictive r^2 can assume a negative value

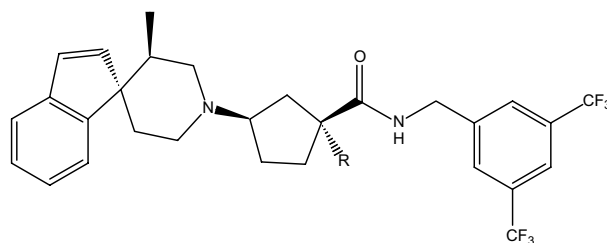
Table 1e. Structure with actual and predicted activity of arylglycinamide class of compounds

S. No.	Molecule	Stereo-isomer	R	IC ₅₀ (nM)	Actual pIC ₅₀	Predicted pIC ₅₀	Residual
25	25	S	3-Thiophene	39	7.41	7.27	0.14
26	26	S	Ph	219	6.66	6.55	0.11
27	27	S	4-F-Ph	175	6.76	6.75	0.01

Table 1f. Structure with actual and predicted activity of α -aminothiazole- γ -aminobutanoic amide class of compounds

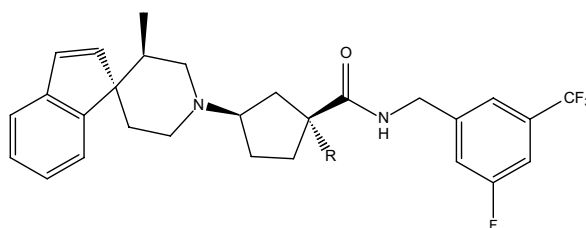
S. No.	Molecule	Stereo-isomer	R	IC ₅₀ (nM)	Actual pIC ₅₀	Predicted pIC ₅₀	Residual
28	28	S	Boc	14.3	7.84	7.64	0.20
29	29	R	Boc	13.3	7.88	7.64	0.24
30	30	S	H	13.3	7.88	8.27	-0.39
31	31*	R	H	229	6.64	7.17	-0.53
32	32	S	COMe	1.8	8.74	8.81	-0.07
33	33*	R	COMe	42	7.38	7.70	-0.32
34	34	S	COOMe	3.5	8.46	8.66	-0.20
35	35	S	CONHMe	0.43	9.37	8.88	0.49
36	36	R	CONHMe	30	7.52	7.83	-0.31

* Test set molecules.

Table 1g. Structure with actual and predicted activity of 3-amino-1-alkyl-cyclopentane carboxamide class of compounds

S. No.	Molecule	R	IC ₅₀ (nM)	Actual pIC ₅₀	Predicted pIC ₅₀	Residual
37	37*	H	20	7.70	7.56	0.14
38	38	Methyl	9	8.05	7.89	0.16
39	39	<i>i</i> -Propyl	7.6	8.12	8.20	-0.08
40	40*	<i>n</i> -Propyl	16	7.80	7.99	-0.19
41	41	<i>i</i> -Butyl	8	8.10	8.07	0.03
42	42	<i>c</i> -Butylmethyl	19	7.72	7.81	-0.09
43	43	CH ₃ SCH ₂ -	13	7.89	8.09	-0.20
44	44	CH ₃ S-	28	7.55	7.56	-0.01

* Test set molecules.

Table 1h. Structure with actual and predicted activity of 3-amino-1-alkyl-cyclopentane carboxamides class of compounds

S. No.	Molecule	R	IC ₅₀ (nM)	Actual pIC ₅₀	Predicted pIC ₅₀	Residual
45	45	Methyl	4	8.40	8.30	0.10
46	46*	<i>i</i> -Propyl	3.1	8.51	8.62	−0.11
47	47	<i>i</i> -Butyl	3.9	8.41	8.48	−0.07
48	48	<i>c</i> -Propyl	1.9	8.72	8.61	0.11
49	49	CH ₃ SCH ₂ −	3.5	8.46	8.51	−0.05
50	50*	CH ₃ S−	67	7.17	7.86	−0.69

* Test set molecules.

Table 2. Statistical parameters obtained for models with different atom counts

Atom-count	1–4	2–5	3–6	4–7	5–8	6–9
r^2 (LOO)	0.709	0.737	0.721	0.761	0.728	0.692
r^2_{ncv}	0.856	0.860	0.853	0.863	0.843	0.825
SE	0.354	0.347	0.358	0.345	0.384	0.391
BHL	353	199	257	199	199	257
NOC	4	4	4	5	5	4

r^2_{ncv} , non-cross validated correlation coefficient; SE, standard error; BHL, best hologram length.; r^2_{cv} , cross-validated correlation coefficient; NOC, number of optimum components.

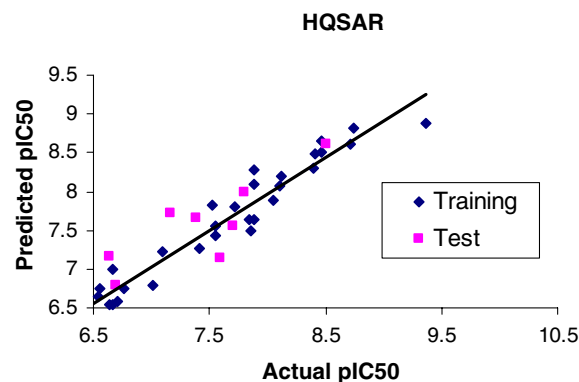
The model chosen for analysis is highlighted in bold fonts.

reflecting a complete lack of predictive ability of the training set.²⁰ The predictive r^2 is defined as given in Eq. 2.

$$r^2_{pred} = (SD - PRESS)/SD \quad (2)$$

where SD is the sum of the squared deviations between the biological activity of molecules in the test set and the mean biological activity of the training set molecules. The PRESS is the sum of the squared deviations between predicted and actual activity values for every molecule in the test set.²¹ It is interesting to note that in the present study that all the 13 molecules of test set were predicted well by the model with a notable predictive r^2 of 0.807. The plot of actual versus predicted pIC₅₀ of the training and test set molecules is shown in Figure 1.

The color coding for a few active molecules representing atomwise contributions is shown in Figure 2. Colors at the red end of the spectrum reflect unfavorable contributions while colors at the green end reflect favorable contributions to CCR2 antagonism. Atoms with intermediate contributions show white color showing their intermediary roles for antagonism. From the color coding one can decipher which particular atom or group is responsible for increase or decrease in the activity. This aids one to further explore and arrive at more potent analogues. For example, replacing the atoms or

**Figure 1.** Plot of actual versus predicted pIC₅₀ of the training and test set molecules by HQSAR analysis. The training set and test set molecules are shown in blue and pink spots, respectively.**Table 3.** Statistical parameters obtained for model with 4–7 atom count

	A	B	Cc	H	C	D & A	r^2_{cv} (LOO)	r^2_{ncv}	SE	BHL	NOC
Model-1	✓	✓	✓				0.761	0.863	0.345	199	5
Model-2	✓	✓	✓	✓			0.563	0.843	0.376	199	5
Model-3	✓	✓	✓		✓		0.837	0.945	0.227	97	6
Model-4	✓	✓	✓			✓	0.697	0.865	0.343	307	4
Model-5	✓	✓	✓	✓	✓	✓	0.697	0.915	0.281	97	6

r^2_{ncv} , non-cross validated correlation coefficient; SE, standard error; BHL, Best Hologram length; r^2_{cv} , cross-validated correlation coefficient; NOC, number of optimum components.

A, atoms; B, bonds; Cc, connections; H, hydrogen atoms; C, chirality; D and A, donor and acceptor.

The model chosen for analysis is highlighted in bold fonts.

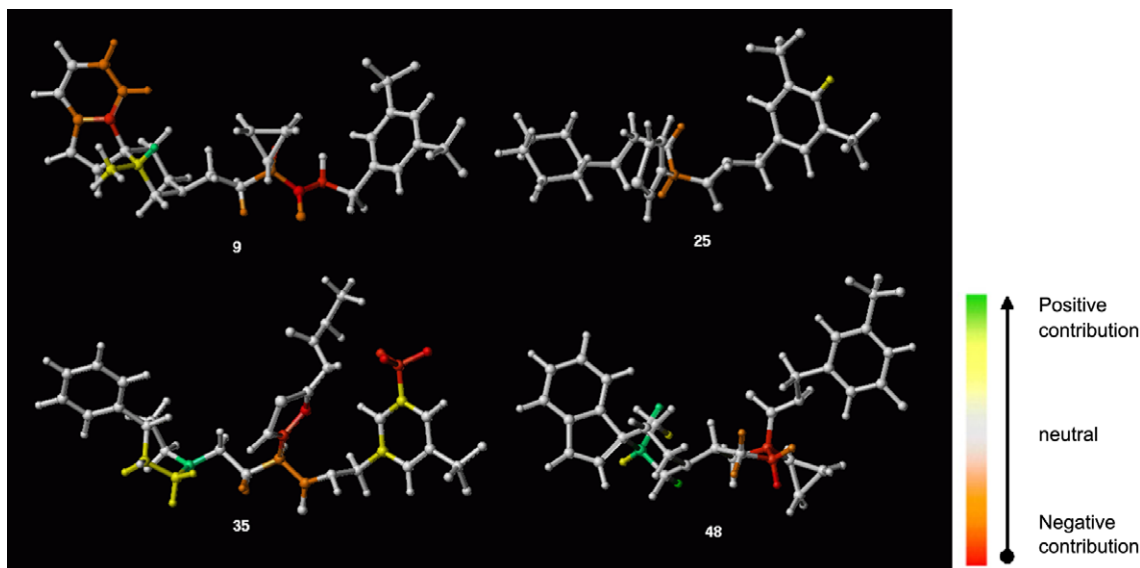


Figure 2. Contribution map giving atom wise contributions for a few most active molecules.

groups with suitable substitutions in red coded regions may increase the binding toward CCR2 for respective class of compounds. A common color trait reflected by red or orange is noted at the chiral center for the potent molecules of the dataset (Fig. 2). This gives an apparent suggestion that satisfactory substitution at asymmetric C atom may increase the binding of respective analogues. For example, presence of a bulky group like 3,5-bis (trifluoromethyl) benzyl linked via amide group at asymmetric center improves CCR2 binding. The piperidine ring nitrogen of aminothiazole class (Fig. 2, 35) shows a green coding and thus suggests its important role for binding with CCR2. The color coding also distinguishes the poorly contributing spiroindenyl (R isomer red-orange) of butyramide class from the intermediary contributing spiroindenyl (S isomer white) of carboxamide series. This suggests the presence of a group with appropriate stereochemistry on left-hand side (Fig. 2, 9, 48) is crucial to increase the binding affinity of compounds. Therefore one can say that spatial orientation of S isomers provides apt complementarities for tight binding with CCR2 compared with the R isomer.

In HQSAR, the molecules are broken down into smaller structural fragments which hold critical information about the activity of the compounds. Thus one can hypothesize the influence of certain fragments for a particular activity. The present study comprises of fragments from the diverse class of CCR2 antagonists and so one can trace out their contribution toward CCR2 antagonism. A few fragments with positive and negative contributions to CCR2 binding are shown in Figure 3. The coefficients of contribution of the generated fragments are in the range of 0.046 to -0.031 . Fragments having positive contributions suggest that they add toward CCR2 binding while those with negative contributions decrease the binding. The analysis of these fragments yields interesting structure–activity relationship (SAR) with the reported data. The analysis of spiro ring shows two different fragments viz., fragment 1 (F1 0.008) and

2 (F2 0.025) with varied contributions. This shows that fragment 1 (F1) may be part of butyramide series which hold R stereo chemistry at spiro region and are less active compared with cyclopentane carboxamide series with S stereochemistry at spiro region.^{15,17} This is also confirmed by the color coding as mentioned above. The SAR studies suggest that *c*-propyl in the S-isomer form gives more potent analogues compared with its R counterpart in butyramide series reflected by fragment 4 (F4 0.013) and fragment 3 (F3 -0.004), respectively.¹⁵ *c*-Butyl analogues are the one among the potent analogues in butyramide class and the fragment (F5) with *c*-butyl feature shows contribution of 0.046.¹⁵ Thus one can generalize that an S-isomer with presence of alicyclic groups is essential for increase in CCR2 antagonism at asymmetric center in butyramide class. A spotting difference in fragment contribution is noted in the aryl glycinamide class of compounds with the 4-methyl piperidinyl analogue (F6 0.003) being more active than the 2-methyl one (F7 -0.008) following the reported activity value.¹⁶ Model failed to distinguish homopiperidinyl with piperidinyl substituted analogue as the fragment contribution of homopiperidinyl (F8 -0.006) is less than the 4-methyl piperidinyl fragment (F6 0.003) even though the homopiperidinyl analogue is more potent.¹⁶ Clear demarcation of fragment contribution for 2-thiophene and 3-thiophene is noted in fragments (F11 -0.008) and (F10 0.010), respectively. The CCR2 binding data of aryl glycinamide series support the fragment analysis as the 3-thiophene analogues were more potent compared to the 2-thiophene analogue.¹⁶ The 4-F phenyl fragment shows less contribution of 0.007 (F9) in contrast to the 3-thiophene fragment. The fragment from most active analogue 35 (S-isomer $IC_{50} = 0.43$ nM) shows a higher contribution over 36 (R-isomer $IC_{50} = 30$ nM) clearly noted with F14 and F15 fragment contributions, respectively.¹⁴

The 2D-QSAR analysis, HQSAR, was used to build statistically significant model with good correlative power

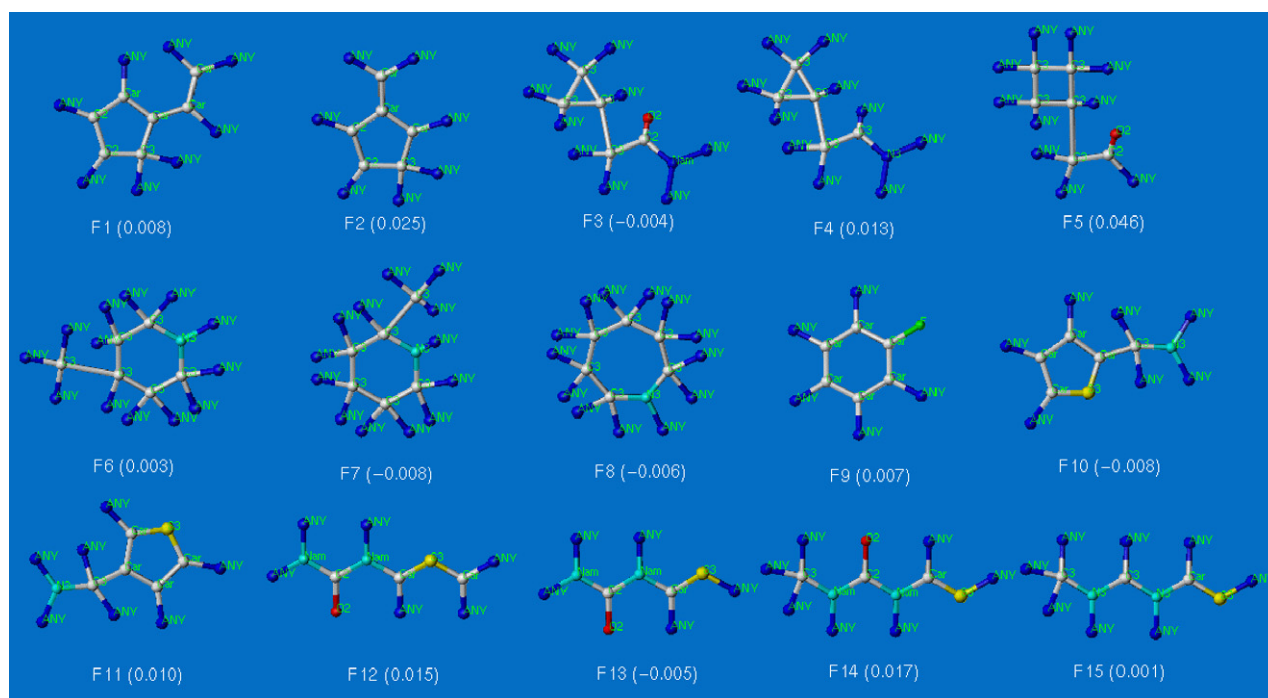


Figure 3. Few fragments with positive and negative contributions to CCR2 antagonism. Color coding for atoms: red (O), grey (C), green (F), cyan (N), yellow (S) and blue (any atom).

for CCR2 antagonists of a diverse set of enantiopure analogues. The best model with atoms, bonds, connectivity, and chirality was significantly more accurate than other models, with $r^2 = 0.945$, $r_{cv}^2 = 0.837$. The robustness of the developed model was verified by external test prediction with r_{pred}^2 of 0.807. In this study, the chirality is the most significant factor that correlated with CCR2 binding. The strong impact of chirality feature based on suitable distinction of R-enantiomers from the S counterparts was observed in derived fragments with their relative contributions. It is noteworthy to say the fragment analysis was in relation with the reported SAR information. And such fragment knowledge can play a key role in understanding the essential pharmacophoric features. The fragment analysis suggests that the asymmetric center bearing amide fragment bonded to a bulky group like aryl or heteroaryl group is very essential for CCR2 binding. Also, from the SAR studies and the fragment analysis it is clear that in general S enantiomers are more potent antagonists compared to their R counterparts. Both fragment and the color codes provide information which can be meaningfully utilized for identification of new scaffolds for CCR2 antagonism. Using this fragment concept we have identified novel scaffolds guided by the HQSAR model prediction and molecular docking studies. The results of this work will be published in due course.

Acknowledgments

This study was conducted using the research facilities available at National Centre for Pharmacoinformatics

(NCPI), established by Department of Science and Technology (DST), Government of India.

References and notes

1. Tsou, C. L.; Peters, W.; Si, Y.; Slaymaker, S.; Aslanian, A. M.; Weisberg, S. P.; Mack, M.; Charo, I. F. *J. Clin. Invest.* **2007**, *117*, 902.
2. Charo, I. F.; Ransohoff, R. M. *N Engl. J. Med.* **2006**, *354*, 610.
3. Lumeng, C. N.; Deyoung, S. M.; Bodzin, J. L.; Saltiel, A. R. *Diabetes* **2007**, *56*, 16.
4. Gu, L.; Tseng, S. C.; Rollins, B. J. *Chem. Immunol.* **1999**, *72*, 7.
5. Newton, R. C.; Vaddi, K. *Methods Enzymol.* **1997**, *287*, 174.
6. Chacon, M. R.; Fernandez-Real, J. M.; Richart, C.; Megia, A.; Gomez, J. M.; Miranda, M.; Caubet, E.; Pastor, R.; Masdevall, C.; Vilarrasa, N.; Ricard, W.; Vendrell, J. *Obesity* **2007**, *15*, 664.
7. Lumeng, C. N.; Bodzin, J. L.; Saltiel, A. R. *J. Clin. Invest.* **2007**, *117*, 175.
8. Barlic, J.; Murphy, P. M. *J. Leukoc Biol.* **2007**, *82*, 226.
9. Oloff, S.; Mailman, R. B.; Tropsha, A. *J. Med. Chem.* **2005**, *48*, 7322.
10. Shen, M.; Beguin, C.; Golbraikh, A.; Stables, J. P.; Kohn, H.; Tropsha, A. *J. Med. Chem.* **2004**, *47*, 2356.
11. Zhang, S.; Wei, L.; Bastow, K.; Zheng, W.; Brossi, A.; Lee, K. H.; Tropsha, A. *J. Comput. Aided Mol. Des.* **2007**, *1*, 97.
12. Zhang, Q.; Muegge, I. *J. Med. Chem.* **2006**, *49*, 1536.
13. Esposito, E. X.; Hopfinger, A. J.; Madura, J. D. *Methods Mol. Biol.* **2004**, *275*, 131.
14. Zhou, C.; Guo, L.; Parsons, W. H.; Mills, S. G.; MacCoss, M.; Vicario, P. P.; Zweerink, H.; Cascieri, M. A.; Springer, M. S.; Yang, L. *Bioorg. Med. Chem. Lett.* **2007**, *17*, 309.

15. Butora, G.; Morriello, G. J.; Kothandaraman, S.; Guida-deen, D.; Pasternak, A.; Parsons, W. H.; MacCoss, M.; Vicario, P. P.; Cascieri, M. A.; Yang, L. *Bioorg. Med. Chem. Lett.* **2006**, *16*, 4715.
16. Yang, L.; Zhou, C.; Guo, L.; Morriello, G.; Butora, G.; Pasternak, A.; Parsons, W. H.; Mills, S. G.; MacCoss, M.; Vicario, P. P.; Zweerink, H.; Ayala, J. M.; Goyal, S.; Hanlon, W. A.; Cascieri, M. A.; Springer, M. S. *Bioorg. Med. Chem. Lett.* **2006**, *16*, 3735.
17. Butora, G.; Jiao, R.; Parsons, W. H.; Vicario, P. P.; Jin, H.; Ayala, J. M.; Cascieri, M. A.; Yang, L. *Bioorg. Med. Chem. Lett.* **2007**, *17*, 3636.
18. SYBYL Molecular Modeling System, version 7.1; Tripos Inc., St. Louis, MO, 63144–2913.
19. Powell, M. J. D. *Math. Program.* **1977**, *12*, 241.
20. Cramer, R. D.; Bunce, J. D.; Patterson, D. E. *Quant. Struct. Act. Relat.* **1988**, *7*, 18.
21. Waller, C. L.; Oprea, T. L.; Giolliti, A.; Marshall, G. R. *J. Med. Chem.* **1993**, *36*, 4152.